Article:
Hébrard, E, Tomlin, AS, Bounaceur, R et al. (2015) Determining predictive uncertainties and global sensitivities for large parameter systems: A case study for N-butane oxidation. Proceedings of the Combustion Institute, 35 (1). pp. 607-616. ISSN: 1873-2704

https://doi.org/10.1016/j.proci.2014.06.027

DETERMINING PREDICTIVE UNCERTAINTIES AND GLOBAL SENSITIVITIES FOR LARGE PARAMETER SYSTEMS: A CASE STUDY FOR N-BUTANE OXIDATION

Éric Hébrard[a], Alison S. Tomlin[b], Roda Bounaceur[a], Frédérique Battin-Leclerc[a*]

[a]Laboratoire Réactions et Génie des Procédés, CNRS - Université de Lorraine, 1 rue Grandville, 54000 Nancy, FRANCE

[b]Energy Research Institute, School of Process Environmental and Materials Engineering, University of Leeds, Leeds, LS2 9JT, UK

Abstract

A global sampling approach based on low discrepancy sequences has been applied in order to propose error bars on simulations performed using a detailed kinetic model for the oxidation of *n*-butane (including 1111 reactions). A two parameter uncertainty factor has been assigned to each considered rate constant. The cases of ignition and oxidation in a jet-stirred reactor (JSR) have both been considered. For the JSR, not only the reactant mole fraction has been considered, but also that of some representative products. A temperature range from 500 to 1250 K has been studied, including the negative temperature coefficient (NTC) region where the predictive error bars have been found to be the largest. It is this temperature region where the highest number of reactions play a role in contributing to the overall output errors. A global sensitivity approach based on high dimensional model representations (HDMR) has then been applied in order to identify those reactions which make the largest contributions to

* To whom correspondence should be addressed. E-mail : Frederique.Battin-Leclerc@univ-lorraine.fr.

the overall uncertainty of the simulated results. The HDMR analysis has been restricted to the most important reactions based on a non-linear screening method, using Spearman Rank Correlation Coefficients at all studied temperatures. The final global sensitivity analysis for predicted ignition delays illustrates that the key reactions are mainly included in the primary mechanism, for temperatures from 700 to 900 K, and in the C_0-C_2 reaction base at higher temperatures. Interestingly, for predicted butane mole fractions in the JSR, the key reactions are almost exclusively from the reaction base, whatever the temperature. The individual contribution of some key reactions is also discussed.

Keywords: Uncertainties, detailed kinetic model, global sampling, global sensitivity, oxidation

INTRODUCTION

The effective use of combustion mechanisms to model and design practical devices requires robust models that can be used in a predictive way over wide ranges of temperatures, pressures and compositions. A measure of the robustness of a model can be obtained by estimating predictive error bars based on our knowledge about the uncertainties within the model parameterization and model structure [1]. However, model error bars are not commonly presented when comparing experimental data with equivalent model simulations. A single comparison is usually made using the best estimates of the model input parameters, with a local sensitivity analysis often applied afterwards to evaluate which parameters most strongly influence the selected target model outputs. Whilst local sensitivities have been used successfully to highlight important parameters within mechanisms for many combustion systems, the estimation of model error bars cannot generally rely on their use. This is particularly true for non-linear models, with input uncertainties that cover large ranges and high

dimensional spaces. For such models, the propagation of uncertainties requires a sampling approach to ensure that all sensitive regions of the input space are covered. Within such an approach, the uncertainties within the inputs are represented by a given distribution (uniform, log-normal etc.), which is then sampled and propagated through the model, providing distributions of the final model predictions. A large number of model runs may be required in order to obtain stable output statistics, such as the mean and variance of the predicted targets. The sampling approach used is critical, since we would like to obtain stable statistics using the lowest possible number of model runs in order to minimize computational costs [2, 3]. Once stable output distributions are obtained, error bars may be calculated using variance based measures (e.g. 1σ or 2σ errors).

We may also wish to determine by how much each of the input parameter uncertainties contributes to the total output variance i.e. to perform an ANOVA (ANalysis Of VAriance) decomposition [4]. Such global sensitivity analyses are also usually based on sampling approaches and could be particularly challenging for large models where the input parameter space is highly multi-dimensional.

In this paper we develop a methodology for estimating error bars for model simulations which incorporate high dimensional combustion mechanisms. Here we focus on uncertainties within the temperature dependent rate coefficients, but the approach could be applied to a wider range of inputs including thermodynamic parameters, transport properties, etc. We use a global sampling approach based on low discrepancy sequences with application to an *n*-butane oxidation model containing 1111 reactions [5, 6]. A screening method is applied based on the calculation of Spearman Rank Correlation Coefficients (RCCs) of this input-output sample, in

order to determine a subset of the main parameters which may affect the final errors over a wide range of conditions. A fully global sensitivity analysis is then performed for this parameter subset using high dimensional model representations (HDMR) [7-9]. We demonstrate that it is possible to achieve an accurate variance decomposition of the output distributions using this two-step approach using reasonably small sample sizes. The work therefore provides a general method for estimating error bars for complex combustion models and obtaining a full ANOVA decomposition of these errors.

METHODOLOGY

Three types of experimental systems are mainly used to provide data for validating detailed gas phase oxidation mechanisms at low-temperatures: rapid compression machines (RCM), shock tubes (ST) and heated flow reactors, such as flow tubes or jet-stirred reactors (JSR). If models are able to reproduce such experimental data over wide ranges of temperatures and pressures, this suggests that the mechanisms may be appropriate for modeling practical combustion devices. However, discrepancies between model predictions and experimental data still exist for certain temperatures and it is therefore important to explore the impact of uncertainties in model input data on the model predictions.

The *n*-butane mechanism used in this study comprises 176 species and 1111 reactions based updates to that proposed in [5] by Bahrini et al. [6]. It is an automatically generated mechanism using the computer package EXGAS, which was previously used to generate oxidation mechanisms for many hydrocarbons and oxygenated fuels [10, 11]. The system provides reaction mechanisms composed of three parts:

1. A comprehensive **primary mechanism**, where the only molecular reactants considered

are the initial organic compounds and oxygen. The following reactions are considered:

- From the initial reactants: production of alkyl radicals through unimolecular and bimolecular initiations, and H atom abstractions by small radicals;
- From alkyl radicals: reactions with O_2 (addition with subsequent reactions of peroxy radicals through isomerizations, second additions to O_2, cyclic ether formations, and disproportionations with HO_2 radicals) or decomposition to alkenes and HO_2 radicals), and isomerizations;
- From all radicals: decompositions of radicals by β-scission involving the breaking of C-C, C=O or C-H bonds.

2. A **C_0-C_2 reaction base**, including all the reactions involving radicals or molecules containing less than three carbon atoms.
3. A lumped **secondary mechanism**, containing the reactions consuming the molecular products of the primary mechanism (e.g ketohydroperoxides, alkenes, cyclic ethers, aldehydes, ketones), which do not react in the reaction base.

Thermochemical data for molecules or radicals are automatically calculated based on group and bond additivity methods. Kinetic data are estimated either based on thermochemical kinetics methods, or on quantitative structure-reactivity relationships obtained from a literature review [11]. The complete mechanism and its associated uncertainties are available as Supplementary Material.

Uncertainty factors were adopted for each rate coefficient and propagated through to determine associated error bars for predictions of ignition delay times in RCMs/ST, and JSR mole fractions. Simulations were performed using CHEMKIN [12] and statistical codes

developed specifically for the present study. RCM/ST simulations were performed using SENKIN assuming a constant volume adiabatic reactor. Whilst this assumption has been questioned for RCM simulations where post compression volume changes may occur due to heat losses, for the shorter ignition delays simulated here this is not expected to have a major influence on the predictions as demonstrated by [13]. JSR simulations have been performed using the PSR code assuming a homogeneous isothermal reactor.

UNCERTAINTY ANALYSIS

Chemical kinetics databases provide recommended values of Arrhenius parameters for many elementary gas-phase reactions, as well as the temperature-dependence of their uncertainties. Ideally, input uncertainties in the temperature-dependence of reaction rates should be described as an analytical expression derived from the covariance matrix of the Arrhenius parameters, as recommended in [14, 15]. However, this is difficult to realize in practice for many large combustion mechanisms where a large number of reactions have not been evaluated. Therefore, we estimate an uncertainty factor $F(T)$ of a reaction rate $k(T)$ at any given temperature following an expression adapted from [16]:

$$F(T) = F(300\text{K}) \cdot g^{\left|\frac{1}{T} - \frac{1}{300}\right|} \qquad (1)$$

where $F(300\text{K})$ is the uncertainty in the rate constant $k(T)$ at $T = 300$ K and g is the "uncertainty-extrapolating" coefficient used to obtain the rate constant uncertainty $F(T)$ at different temperatures. The approach is based on the fact that rate constants are almost always known with a minimum uncertainty at room temperature, but allows us to quantify the temperature-dependent uncertainties over a temperature range adequate for combustion studies. Uncertainty factors $F(T)$ were assigned to each temperature-dependent rate constant, (1111 parameters here)

using appropriate evaluation studies where available. This is mostly the case for the C_0-C_2 reaction base, where many reviews provide temperature-dependent uncertainties assuming that the minimum and maximum values of the rate coefficients correspond to 1σ [16], 2σ [18] or 3σ [17] deviations from the recommended value on a logarithmic scale. For example, Baulch et al. [17] recommended uncertainties for the rate of the reaction $H + O_2 = O + OH$ (reaction 927) as $F(300K) = 1.08$ and $F(5000K) = 1.47$, giving $F(300K) = 1.08$ and $g = 100$ over the temperature range 300-5000 K. For the calculated parameters within the primary and secondary mechanisms, factors $F = 1.26$, $g = 0$ were used for unimolecular or bimolecular initiations and additions with oxygen, whereas $F = 1.12$, $g = 100$ were used otherwise.

Because of the highly non-linear nature of combustion models and their potentially large ranges of uncertainties, a linear uncertainty propagation is not expected to produce valid results. Propagation of distributions by random sampling across the whole space spanned by the input distributions is better adapted to such problems [19]. Due to the positivity constraint on these properties, their distributions are modeled by lognormal probability density functions:

$$f(x) = \frac{1}{\sqrt{2\pi}\sigma x} \exp\left[-\frac{(\ln x - \mu)^2}{2\sigma^2}\right] \qquad (2)$$

with $\mu = \ln k(T)$, the logarithm of the nominal value of the reaction rate at temperature T, and $\sigma = \ln F(T)$, the logarithm of the geometric standard uncertainty $F(T)$ of the lognormal distribution. With these notations, the 67% confidence interval for a reaction rate at a given temperature is given as $[k(T)/F(T),\ k(T)\times F(T)]$. Adopted F values are supplied with the mechanism in the Supplementary Material and represent 1σ values. Within the uncertainty analysis 3σ errors were propagated in order to encompass most possible values of the rate constants (99.7% confidence limits) and hence F=1.26 at 1σ equates to a factor of 2 uncertainty

at 3σ. A fuller description is given in Supplementary Material. For many reactions, particularly those from the primary and secondary mechanisms, these uncertainties have to be estimates since there is insufficient experimental or theoretical data from which to perform a full evaluation. The adopted uncertainties will inevitably affect the variance decomposition and this should be noted in the interpretation of the global sensitivity results.

Many different sampling methods have been used for sensitivity and uncertainty analysis [20]. Monte Carlo methods are commonly used and involve generating a large number of independent random parameter sets that correspond to the joint probability density function of model inputs or cover their feasible region using a given distribution. Subsequently model simulations are carried out for each set and the scatter or distributions in the target model outputs are investigated. Random sampling forms the standard method, but with the possible disadvantage of clustering occurring in some regions of the input space and gaps in other regions. A possible alternative is the use of low discrepancy sequences. Discrepancy is a measure of the uniformity of a sequence; high uniformity equals low discrepancy. Successive sample points are added to positions as far away as possible from existing sample points so that clustering can be avoided. One of the best known low discrepancy sequences was proposed by Sobol [21][1].

A normal distribution of random numbers can be obtained from a uniform distribution of random numbers using the Box-Muller algorithm (e.g., [22]). However, for low discrepancy sequences, it should be avoided because it may damage their intrinsic properties, either by altering the order of the sequence or by scrambling the sequence uniformity [23, 24]. We

[1] SOBOL library : original FORTRAN77 version by Bennett Fox; FORTRAN90 version by John Burkardt : http://people.sc.fsu.edu/~jburkardt/f src/sobol/sobol.html

therefore compute directly the inverse normal distribution of the Sobol sequence given its cumulative distribution function[2].

Fig. 1 displays a comparison of samples obtained from a uniform pseudo-random distribution and a Sobol sequence for a 2-parameter sample where the sample size N=1000. The Sobol sequence provides a more uniform coverage compared to the random sample. Clustering and gaps are visible for the random sample even within two dimensions, and for small sample sizes (~1000) these could become quite extreme within a 1111 dimensional space as studied here. However, using a Sobol sequence we found that the variance of the model outputs achieved convergence even using a small sample size of 1000, in agreement with previous work that evaluated the convergence properties of different sampling strategies [3].

After a quasi-random sample is drawn from the input distribution, the autoignition delay times and the JSR mole fractions are predicted for each member of this quasi-random sample. Error bars on simulations represented by 1σ bands vs. temperature are shown in Fig. 2 in the case of autoignition, and in Fig. 3 in the case of JSR mole fractions. For the JSR, simulations were performed under the conditions of [6] (Φ=1, P=1atm, T=500−1000K, t=6s). Simulated autoignition delay times in air were performed using the conditions of [25] (Φ=1, P=10 atm, T=700−1300K). The related experimental results are also shown for comparison. To indicate the experimental uncertainty, several literature experimental ignition delays times obtained under conditions close to those of [25] are also plotted in Fig. 3.

[2] NORMINV: An algorithm for computing the inverse normal cumulative distribution function. Based on Peter John Acklam's algorithm : http://home.online.no/p~jacklam/notes/invnorm/

Fig. 2 shows that the error bars are largest (up to a factor of 8) in the NTC region (750-850 K) and are larger than the scatter in experimental data from various sources. Above 850 K, these error bars significantly decrease, to around a factor of 2. Fig. 3 shows predicted means and confidence intervals for the mole fractions of the reactant in the JSR, as well as for 5 representative products. Aldehydes and ethylene are considered as good indicators of low and high temperature reactivity, respectively. Butenes and 2-methyloxetane are amongst the important primary products. As for ignition, the error bars related to the reactivity are largest in the NTC region, as indicated by the reactant and aldehyde mole fractions. The errors for ethylene are especially large above 900 K. Also note that the error bars for the cyclic ether are perhaps lower than would be expected from the usual level of agreement found between simulations and experiments for this family of compounds [26]. The simulated error bars and data points do not overlap in Fig. 3. This could be due to a number of reasons including experimental error, even for compounds with the largest experimental uncertainty such as CH_2O [6] (see given experimental error bars), but a likely reason is that the adopted uncertainty factors for some reactions in the primary mechanism were perhaps too optimistic. The influence of input parameter uncertainty estimation, especially in the primary and secondary mechanisms, on predicted error bars should certainly be more thoroughly investigated in future work.

GLOBAL SENSITIVITY ANALYSIS

Global sensitivity analysis was then performed at various temperatures in order to provide a variance decomposition of the error bars shown in the previous figures. Butane was chosen as being representative of the overall reactivity of the oxidation scheme for the JSR simulations. **A** two-step process was used, since performing a variance decomposition within a 1111 dimensional space is unlikely to lead to high fidelity results without resorting to very large

sample sizes with associated computational costs. A screening method was therefore first used in order to pre-select those parameters which are likely to contribute to the overall variance of the model predictions. Whilst linear sensitivity analysis is commonly used as pre-screening step, it was not used here since the response of the predicted outputs to changes in inputs may not be linear across the input uncertainty ranges. Focusing calculations around the nominal parameter values may therefore give misleading results [8]. A global screening approach based on Spearman Rank Correlation Coefficients (RCCs) was therefore adopted using the input-output distributions built from the original Sobol sequences.

RCCs [31] provide a measure of the strength of the non-linear relationship between model inputs and target outputs, by assessing how well the relationship between two variables can be described using a monotonic function. The RCC threshold was set to 0.2 to give a reasonable yet restricted set of significant reactions as shown in Table 1 for simulated autoignition delay times and butane mole fractions in the JSR. 29 key reactions were identified for ignition delays and 34 for the JSR mole fractions. These inputs were then selected for the subsequent global sensitivity analysis.

A further Sobol sequence was then generated for these restricted sets of inputs and checks were made to ensure that the total predicted output variance from this restricted sample was well matched to that from the original sample where all 1111 parameters were varied. This provides confidence that a successful screening was performed and that the following variance decomposition accurately provides the importance of each parameter in terms of its contribution to output uncertainties discussed above.

The global sensitivity study was performed using a high dimensional model representation (HDMR) method based on a hierarchical expansion of the input-output relationship generated from the Sobol sample as described in [9]. Using HDMR, variance based sensitivity indices can be determined in an automatic way from the hierarchical function expansion, hence providing a ranking of each parameter in terms of its contribution to the predicted output variance.

Fig. 4 displays the global first-order sensitivity indices calculated for ignition delays every 50 K from 700 to 1300 K. Two excel files in Supplementary Material present the results in more detail for ignition and PSR results, respectively. The analyzed reactions are numbered as shown in Table 1. If a full variance decomposition is achieved then the sum of the sensitivities should be 1. Second-order indices were calculated but are not shown here for simplicity of interpretation. The white parts in Fig. 4 and in the boxes of Fig. 5 correspond to these and potentially higher order effects. Based on the first order terms from the ANOVA analysis, Fig. 5 presents how the error bars shown in Figs. 2 and 3 are decomposed into contributions attributable to reactions included in the primary mechanism, the secondary mechanism, and the reaction base, respectively. For autoignition delay times, Figs. 4 and 5(a) highlight, as expected, the importance of reactions of the primary mechanism up to 900 K whilst at higher temperatures reactions from the C_0-C_2 reaction base dominate. Whilst the input uncertainties for reactions of the secondary mechanism are certainly large, their contribution to output uncertainty is very small and only significant below 1000 K. This supports the lumping approach used in the generation of secondary mechanisms by the EXGAS software [11]. Perhaps more surprisingly, Fig. 5(b) indicates that the JSR simulations are almost exclusively dominated by uncertainties in reactions from the C_0-C_2 base, even at low temperatures. As shown in Supplementary Material, at 550 K, the

isomerization of one of the butylperoxy radicals (reaction 26 in Table 1) is the only identified contributor to the error bar, and at 600 K, the reactions of radicals derived from ethyl radicals (e.g reaction 897), which are mainly obtained from ketohydroperoxides decomposition, have a significant contribution. However at higher temperature only reactions of HO_2, CH_3, HCHO, and to minor extent CH_3CHO have a notable contribution. Further studies of these reactions could help to improve the predictability of the mechanism.

In Fig. 4 and better shown in Supplementary Material, under ignition conditions below 800 K, the reactions with the highest contributions are the isomerizations of both butylperoxy radicals (reactions 22 and 26) and oxidation to give butene and HO_2 radicals from butyl radicals (reactions 153-155). Above 900 K, the contribution of the metathesis of butane with HO_2 radicals (reactions 207 and 208) and of the combination of methyl and HO_2 radicals (reaction 977) start to be significant, with the contribution of these last reactions being dominant for all temperatures above 1050 K. A notable contribution of the formation of H_2O_2 from HO_2 radicals (reaction 998) appears from 950 to 1050 K, and finally one of the reaction $H + O_2 = O + OH$ (reaction 927) starts from 1150 K, confirming the determinant role of branching steps in ignition.

CONCLUSION

We have demonstrated a computationally efficient method for providing predictive error bars on combustion simulations using complex reaction mechanisms, based on a sampling approach using low discrepancy sequences. The variance decomposition of these errors provides information on those reactions requiring further study in order to improve the robustness of the model simulations i.e. to reduce the error bars. This variance decomposition was achieved in a

two-step process using a prior screening of the parameters using Spearman Rank Correlation Coefficients, followed by HDMR analysis for the selected parameters to estimate global sensitivity indices. When applied to simulations of experimental data obtained from RCM, shock tube and a JSR for *n*-butane oxidation, the results provide a highly visual way to evaluate how the sensitivities to uncertainties within the mechanism change across the different temperature regimes. Very little sensitivity to the secondary mechanism was observed across all temperature ranges for all reactor studies. Sensitivities to the reactions within the primary butane scheme were mainly observed for the low temperature ignition delay experiments, suggesting that such experiments could provide useful constraints on the R+O_2, and RO_2 to QOOH isomerization pathways if used within an optimization approach. Perhaps surprisingly, the predicted butane mole fractions within the JSR simulations were mainly sensitive to reactions within the base scheme, particularly reactions involving HO_2, HCHO, CH_3, and to a minor extent C_2H_5 or CH_3CHO.

ACKNOWLEDGEMENT

This work was supported by the European Commission through the "Clean ICE" Advanced Research Grant of the European Research Council and by COST Action CM0901.

3 SUPPLEMENTARY MATERIALS

1/ Mechanism and uncertainties (pdf file)

2/ SI_results_HDMR_SENKIN (excel.file)

3/ results_HDMR_PSR (excel.file)

REFERENCES

[1] A. S. Tomlin, Proc. Combust. Inst. 34 (2013) 159–176.

[2] A. Saltelli, M. Ratto, T. Andres, F. Campolongo, J. Cariboni, D. Gatelli, M. Saisana, S. Tarantola, Global sensitivity analysis: The primer, WileyInterscience, Wiley, 2008.

[3] A. S. Tomlin, T. Ziehn, in: A. Gorban, D. Roose (Eds.), Coping with complexity: Model reduction and data analysis, Lecture notes in computational science and engineering, Springer, 2011, pp. 9–36.

[4] I. Sobol, Math. Comput. Simulat. 55 (2001) 271–280.

[5] F. Battin-Leclerc, O. Herbinet, P.-A. Glaude, R. Fournet, Z. Zhou, L. Deng, H. Guo, M. Xie, F. Qi, Proc. Combust. Inst. 33 (2011) 325–331.

[6] C. Bahrini, P. Morajkar, C. Schoemaecker, O. Frottier, O. Herbinet, P.A. Glaude, F. Battin-Leclerc, C. Fittschen, Phys. Chem. Chem. Phys. 15 (2013) 19686–19698.

[7] T. Ziehn, A. S. Tomlin, Int. J. Chem. Kinet. 40 (2008) 742–753.

[8] T. Ziehn, K. J. Hughes, J. F. Griffiths, R. Porter, A. S. Tomlin, Combust. Theo. Model. 13 (2009) 589–605.

[9] T. Ziehn, A. S. Tomlin, Environ. Modell. Softw. 24 (2009) 775–785.

[10] F. Buda, R. Bounaceur, V. Warth, P. Glaude, R. Fournet, F. BattinLeclerc, Comb. Flame 142 (2005) 170–186.

[11] E. Blurock, F. Battin-Leclerc, in: F. Battin-Leclerc, J. M. Simmie, E. Blurock (Eds.), Cleaner Combustion, Green Energy and Technology, Springer London, 2013, pp. 17–57.

[12] R. J. Kee, F. M. Rupley, J. A. Miller, Chemkin II: A FORTRAN chemical kinetics package for the analysis of gasphase chemical kinetics, Technical Report SAND89-8009B, Sandia National Laboratories, 1993.

[13] Z. Serinyel, O. Herbinet, O. Frottier, P. Dirrenberger, V. Warth, P.A. Glaude, F. Battin-Leclerc, Combust. Flame 160 (2013) 2319.

[14] E. Hébrard, M. Dobrijevic, P. Pernot, N. Carrasco, A. Bergeat, K. M. Hickson, A. Canosa, S. D. Le

Picard, I. R. Sims, J. Phys. Chem. A 113 (2009) 11227–11237.

[15] T. Nagy, T. Turányi, Int. J. Chem. Kinet. 43 (2011) 359–378.

[16] S. P. Sander, J. Abbatt, J. R. Barker, J. B. Burkholder, R. R. Friedl, D. M. Golden, R. E. Huie, C. E. Kolb, M. J. Kurylo, G. K. Moortgat, V. L. Orkin, P. H. Wine, JPL Publication 10-6 (2011).

[17] D. L. Baulch, C. T. Bowman, C. J. Cobos, R. A. Cox, T. Just, J. A. Kerr, M. J. Pilling, D. Stocker, J. Troe, W. Tsang, R. W. Walker, J. Warnatz, J. Phys. Chem. Ref. Data 34 (2005) 757–1397.

[18] R. Atkinson, D. L. Baulch, R. A. Cox, J. N. Crowley, R. F. Hampson, R. G. Hynes, M. E. Jenkin, M. J. Rossi, J. Troe, T. J. Wallington, Atmos. Chem. Phys. 8 (2008) 4141–4496.

[19] BIPM, IEC, IFCC, ISO, IUPAC, IUPAP, OIML, Evaluation of measurement data Supplement 1 to the GUM: Propagation of distributions using a Monte-Carlo method, Technical Report, BIPM, 2006.

[20] J. Helton, J. Johnson, C. Sallaberry, C. Storlie, Reliab. Eng. Syst. Saf. 91 (2006) 1175–1209.

[21] I. Sobol, USSR Comput. Math. Math. Phys. 7 (1967) 86–112.

[22] W. Press, S. Teukolsky, W. Vetterling, B. Flannery, Numerical recipes in Fortran. The art of scientific computing, Cambridge University Press, 1992.

[23] B. Moro, Risk 8 (1995) 57–58.

[24] S. Galanti, A. Jung, J. Deriv. 5 (1997) 63–83.

[25] D. Healy, N. Donato, C. Aul, E. Petersen, C. Zinner, G. Bourque, H. Curran, Comb. Flame 157 (2010) 1526–1539.

[26] M. Cord, B. Sirjean, R. Fournet, A. Tomlin, M. Ruiz-Lopez, F. BattinLeclerc, J. Phys. Chem. A 116 (2012) 6142–6158.

[27] M. Carlier, C. Corre, R. Minetti, J.-F. Pauwels, M. Ribaucour, L.-R. Sochet, Symp. Int. Combust. Proc. 23 (1991) 1753–1758.

[28] R. Minetti, M. Ribaucour, M. Carlier, C. Fittschen, L. Sochet, Comb. Flame 96 (1994) 201–211.

[29] R. Minetti, M. Ribaucour, M. Carlier, L. Sochet, Combust. Sci. Technol.113 (1996) 179–192.

[30] J. Griffiths, P. Halford-Maw, D. Rose, Comb. Flame 95 (1993) 291–306.

[31] C. Spearman, Am. J. Psychol. 15 (1904) 72–101.

Table 1: Key reactions during the simulations of the autoignitition delay times with SENKIN [S] and of the oxidation of n-butane with PSR [P]. Reactions are numbered in the first column as in the mechanism (see Supporting Information).

N°	Reactions	S	P
6	$1\text{-}C_4H_9+O_2 \rightarrow C_4H_9{-}1{-}OO$		1
7	$2\text{-}C_4H_9+O_2 \rightarrow C_4H_9{-}2{-}OO$		2
22	$C_4H_9{-}1{-}OO \rightarrow C_4H_8{-}1{-}OOH$	1	
26	$C_4H_9{-}2{-}OO \rightarrow C_4H_8{-}_2{-}OOH$	2	
81	$2\text{-}C_4H_7{-}13{-}(OOH)_2 \rightarrow HO_2+C_4H_7OOH$	3	
131	$2\text{-}C_4H_7{-}34{-}(OOH)_2 \rightarrow OH+_2\text{-methoxy-1,3-dioxolane}$		4
132	$1\text{-}C_4H_7{-}34{-}(OOH)_2 \rightarrow OH+_2\text{-methoxy-1,3-dioxolane}$	4	
153	$1\text{-}C_4H_9+O_2 \rightarrow 1\text{-}C_4H_8+HO_2$	5	
154	$2\text{-}C_4H_9+O_2 \rightarrow 1\text{-}C_4H_8+HO_2$	6	5
155	$2\text{-}C_4H_9+O_2 \rightarrow 1\text{-}C_4H_8+HO_2$	7	
177	$1\text{-}C_4H_7{-}_{24}{-}(OOH)_2+O_2 \rightarrow 1\text{-}C_4H_6\text{-}2,4,\text{-}(OOH)_2+HO_2$	8	
204	$C_4H_{10}+H \rightarrow H_2+2\text{-}C_4H_9$	9	
205	$C_4H_{10}+OH \rightarrow H_2O+1\text{-}C_4H_9$	10	
206	$C_4H_{10}+OH \rightarrow H_2O+2\text{-}C_4H_9$	11	
207	$C_4H_{10}+HO_2 \rightarrow H_2O_2+1\text{-}C_4H_9$	12	
208	$C_4H_{10}+HO_2 \rightarrow H_2O_2+2\text{-}C_4H_9$	13	
256	$CH_3C(O)C_2H_4OOH \rightarrow OH+CH_3C(O)C_2H_4O$		6
282	$C_3H_8+CH_3 \rightarrow CH_4+1\text{-}C_3H_7$	14	7
291	$C_5H_{12}+HO_2 \rightarrow H_2O_2+CH_3+C_2H_4+C_2H_4$	15	
297	$C_5H_{12}+C_2H_5 \rightarrow C_2H_6+CH_3+C_2H_4+C_2H_4$		8
314	$\text{methyloxirane}+OH \rightarrow H_2O+CH_3+CH_2CO$		9
344	$\text{propyloxirane}+OH \rightarrow H_2O+1\text{-}C_3H_7+CH_2CO$		10
353	$\text{methylpropyloxirane}+H \rightarrow H_2+1\text{-}C_3H_7+C_2H_3CHO$	16	
364	$\text{methylpropyloxirane}+C_2H_5 \rightarrow C_2H_6+1\text{-}C_3H_7+C_2H_3CHO$		11
425	$C_5H_{10}+OH \rightarrow CH_3+C_3H_7CHO$	17	
444	$C_5H_{10}+H \rightarrow H_2+13{-}C_4H_6+CH_3$		12
454	$C_5H_{10}+CH_3 \rightarrow CH_4+13{-}C_4H_6+CH_3$	18	
470	$C_6H_{12}+CH_3 \rightarrow CH_4+13{-}C_4H_6+C_2H_5$	19	13
497	$C_3H_6+O \rightarrow C_3H_5+OH$	20	14
509	$C_3H_7OH+HO_2 \rightarrow H_2O_2+OH+C_3H_6$	21	
545	$C_2H_5CHO+HO_2 \rightarrow H_2O_2+C_3H_5O$		15
570	$C_5H_9O \rightarrow CO+1\text{-}C_4H_9$		16
587	$C_3H_7CHO+HO_2 \rightarrow H_2O_2+CH_2CO+C_2H_5$		17
652	$CH+H \rightarrow C+H_2$	22	
704	$C_2H_6+C_2H \rightarrow C_2H_2+C_2H_5$		18
730	$H+O+M \rightarrow OH+M$		19
780	$HCHO+H \rightarrow HCO+H_2$	23	20
837	$CH_3OH+OH \rightarrow CH_3O+H_2O$		21
845	$HCCO+OH \rightarrow HCO+CO+H$	24	
897	$C_2H_5O \rightarrow HCHO+CH_3$		22
911	$C_2H_5OH+O_2 \rightarrow C_2H_4{-}1{-}OH+HO_2$		23
927	$O_2+H \rightarrow OH+O$	25	24
977	$HO_2+CH_3 \rightarrow CH_3O+OH$	26	25
990	$HO_2+HCHO \rightarrow HCO+H_2O_2$		26
995	$HO_2+CH_3CHO \rightarrow CH_3CO+H_2O_2$		27
997	$HO_2+HO_2 \rightarrow H_2O_2+O_2$		28
998	$HO_2+HO_2 \rightarrow H_2O_2+O_2$	27	29
999	$H_2O_2(+M) \rightarrow OH+OH(+M)$	28	
1038	$CH_3O_2+H_2O_2 \rightarrow CH_3OOH+HO_2$		30
1041	$CH_3OOH \rightarrow CH_3O+OH$		31
1055	$C_2H_5OO+HCHO \rightarrow C_2H_5OOH+HCO$		32
1071	$C_2H_5OOH \rightarrow C_2H_5O+OH$		33
1073	$C_2H_5OOH+CH_3 \rightarrow CH_3CHO+OH+CH_4$	29	34

FIGURE CAPTIONS

Figure 1: A comparison of distributions for different sampling strategies for a 2-parameters sample with N = 1000. Uniform pseudo- random sample (top left), Sobol's quasi-random sequence sample (top right), Box-Muller transformation applied to an uniform pseudo-random sample (bottom left) and the normal inverse cumulative function of a Sobol's quasi-random sequence sample (bottom right).

Figure 2: Predictions of the autoignition delay times vs. temperature. Black solid line: nominal and mean profile. Blue-filled area corresponds to the standard deviation (1σ) of the modeled results. STD = shock-tube data. RCM = rapid compression machine [25,27,28,30].

Figure 3: Predictions of the mole fraction profiles vs. temperature of some representative products during the oxidation of n-butane in a JSR. Black solid lines: nominal and mean.profiles. Blue-filled area corresponds to the standard deviation (1σ) of the modeled results. Red squared symbols are GC measurements [6].

Figure 4: Normalized estimates of first-order contributions to the overall variance of predicted autoignition delay times vs. temperature calculated using the global HDMR method under the conditions of Fig. 2. Reactions are numbered on the boxplot as in the mechanism (see Supporting Information) but the colormap has been scaled to the limited set of reactions numbered and ordered as specified in the third column of the Table 1.

Figure 5: Predictions of autoignition delay times and C_4H_{10} mole fraction profiles vs. temperature under the conditions of Figs. 2 (left) and 3(a) (right). The boxplots display the

observed variance in a particular variable is partitioned into components attributable to different chemical sources of variation in the mechanism [6]: primary mechanism (blue), secondary mechanism (green), C0-C2 base (red).

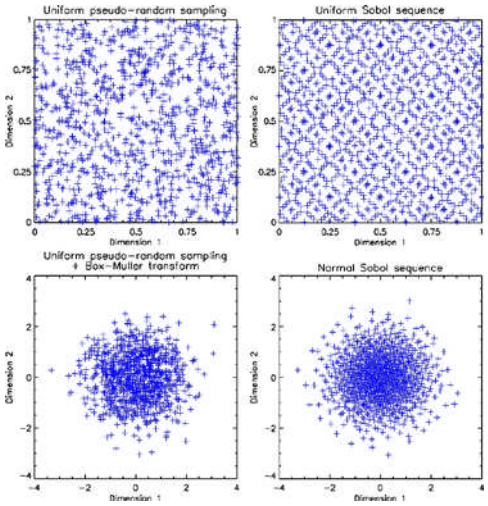

Figure 1: A comparison of distributions for different sampling strategies for a 2-parameters sample with N = 1000. Uniform pseudo- random sample (top left), Sobol's quasi-random sequence sample (top right), Box-Muller transformation applied to an uniform pseudo-random sample (bottom left) and the normal inverse cumulative function of a Sobol's quasi-random sequence sample (bottom right).

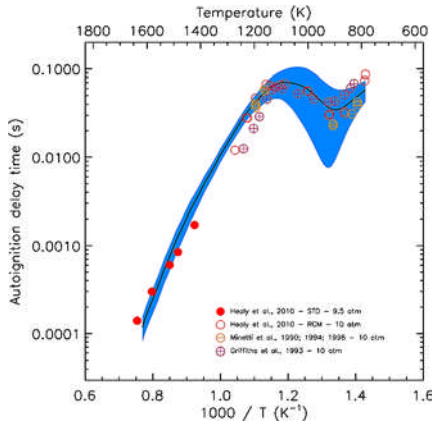

Figure 2: Predictions of the autoignition delay times vs. temperature. Black solid line: nominal and mean profile. Blue-filled area corresponds to the standard deviation (1σ) of the modeled results. STD = shock-tube data. RCM = rapid compression machine [25,27,28,30].

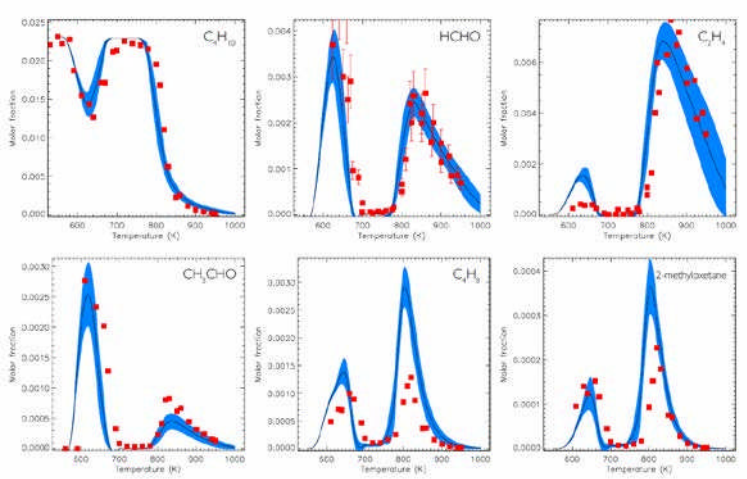

Figure 3: Predictions of the mole fraction profiles vs. temperature of some representative products during the oxidation of n-butane in a JSR. Black solid lines: nominal and mean.profiles. Blue-filled area corresponds to the standard deviation (1σ) of the modeled results. Red squared symbols are GC measurements [6].

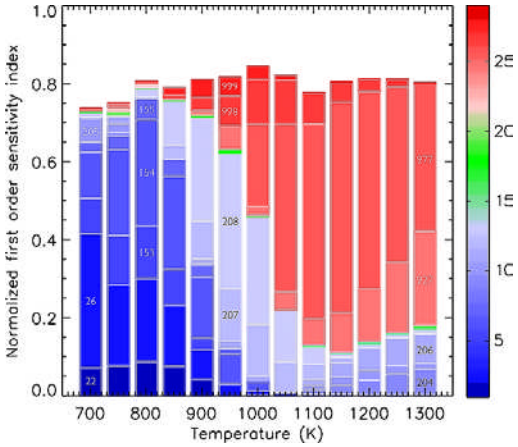

Figure 4: Normalized estimates of first-order contributions to the overall variance of predicted autoignition delay times vs. temperature calculated using the global HDMR method under the conditions of Fig. 2. Reactions are numbered on the boxplot as in the mechanism (see Supporting Information) but the colormap has been scaled to the limited set of reactions numbered and ordered as specified in the third column of the Table 1.

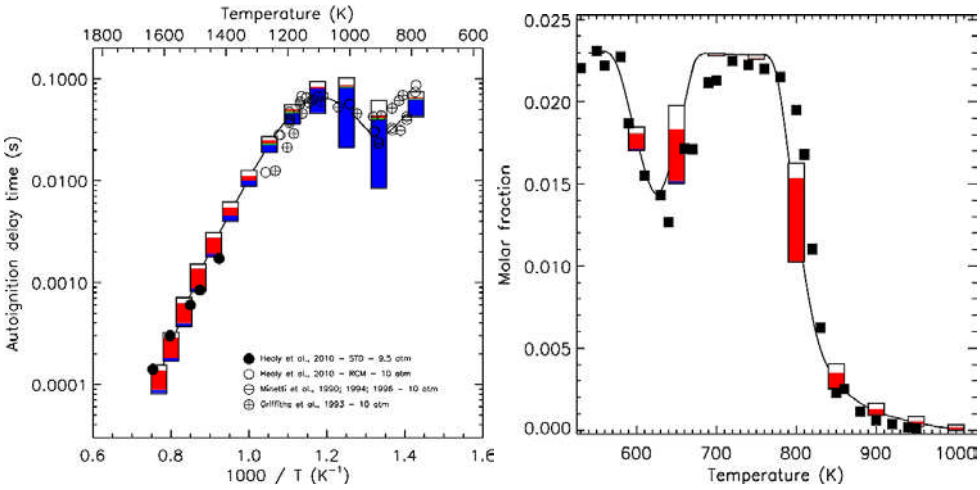

Figure 5: Predictions of autoignition delay times and C_4H_{10} mole fraction profiles vs. temperature under the conditions of Figs. 2 (left) and 3(a) (right). The boxplots display the observed variance in a particular variable is partitioned into components attributable to different chemical sources of variation in the mechanism [6]: primary mechanism (blue), secondary mechanism (green), C0-C2 base (red).